Journal of Molecular Structure 1059 (2014) 193–201

Contents lists available at ScienceDirect

Journal of Molecular Structure

journal homepage: www.elsevier.com/locate/molstruc

Zinc(II), ruthenium(II), rhodium(III), palladium(II), silver(I), platinum(II) and MoO_2^{2+} complexes of 2-(2′-hydroxy-5′-methylphenyl)-benzotriazole as simple or primary ligand and 2,2′-bipyridyl, 9,10-phenanthroline or triphenylphosphine as secondary ligands: Structure and anticancer activity

Hala A. El-Asmy [a], Ian S. Butler [a,*], Zhor S. Mouhri [b], Bertrand J. Jean-Claude [b], Mohamed S. Emmam [c], Sahar I. Mostafa [c,*]

[a] Department of Chemistry, McGill University, Montreal, QC H3A 2K6, Canada
[b] Royal Victoria Hospital, Department of Medicine, McGill University, Montreal, QC H3A 1A1, Canada
[c] Chemistry Department, Faculty of Science, Mansoura University, Mansoura 35516, Egypt

HIGHLIGHTS

- New complexes of 2-(2′-hydroxy-5′-methylphenyl)-benzotriazole (Hhmbt) are reported.
- Hhmbt coordinates via deprotonated hydroxy and imine nitrogen.
- Free Hhmbt and its complexes were tested against breast cancer (MDA-MB231) and ovarian cancer (OVCAR-8) cell lines.
- [Ag(hmpbt)(PPh_3)] and [Pd(phen)(hmbt)]Cl exhibit the highest activity.

GRAPHICAL ABSTRACT

New complexes of 2-(2′-hydroxy-5′-methylphenyl)-benzotriazole have been synthesized and structurally characterized. The reported complexes have been tested against human breast cancer (MDA-MB231) and human ovarian cancer (OVCAR-8) cell lines.

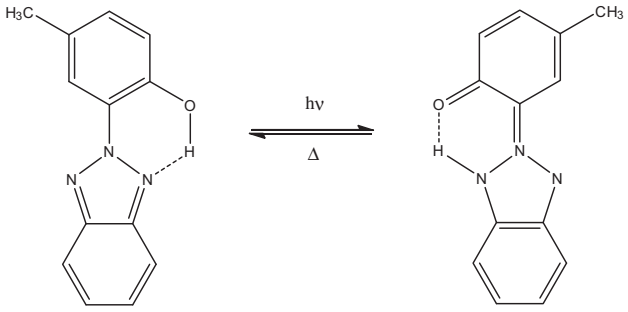

ARTICLE INFO

Article history:
Received 1 October 2013
Received in revised form 14 November 2013
Accepted 14 November 2013
Available online 23 November 2013

Keywords:
Hhmbt
Zinc
Palladium
Platinum
Silver
Anticancer

ABSTRACT

New complexes of 2-(2′-hydroxy-5′-methylphenyl)-benzotriazole (Hhmbt), [Zn(hmbt)$_2$(H_2O)$_2$], [Zn(hmbt)(OAc)(H_2O)$_2$], [Pd(hmbt)(H_2O)Cl], [Pd(hmbt)$_2$], [M(PPh_3)(hmbt)Cl], [M(L)(hmbt)]Cl (M(II) = Pd, Pt; L = bpy, phen), [Ag_2(hmbt)$_2$], [Ag(phen)(hmbt)], [Ag(PPh_3)(hmbt)], [Rh(hmbt)$_2$(H_2O)$_2$]Cl, [Ru(hmbt)$_2$(H_2O)$_2$], [Ru(PPh_3)(hmbt)$_2$Cl] and *cis*-[MoO_2(hmbt)$_2$] have been synthesized. They have been structurally and spectroscopically characterized on the basis of elemental analysis, IR, NMR (^{1}H, ^{13}C, ^{31}P), UV–vis. and ESI-mass spectroscopy, thermal and molar conductivity measurements. 2-(2′-Hydroxy-5′-methylphenyl)-benzotriazole behaves as a mononegative bidentate through the deprotonated phenolic oxygen and imine nitrogen atoms. The reported complexes have been tested against human breast cancer (MDA-MB231) and human ovarian cancer (OVCAR-8) cell lines. The complexes, [Ag(hmpbt)(PPh_3)], [Rh(hmbt)$_2$(H_2O)$_2$]Cl, [Pt(phen)(hmbt)]Cl and [Pd(phen)(hmbt)]Cl exhibit the highest growth inhibitory activity with mean IC_{50} values 1.37, 7.52, 5.24 and 4.85 μM (MDA-MB231) and 1.75, 8.50, 3.00 and 2.99 μM (OVACAR-8), respectively.

* Corresponding authors. Tel.: +20 100 8502625; fax: +20 50 2246781.
E-mail addresses: ian.butler@mcgill.ca (I.S. Butler), sihmostafa@yahoo.com (S.I. Mostafa).

0022-2860/$ - see front matter Crown Copyright © 2013 Published by Elsevier B.V. All rights reserved.
http://dx.doi.org/10.1016/j.molstruc.2013.11.039

1. Introduction

2-(2′-Hydroxy-5′-methylphenyl)-benzotriazole (Fig. 1) is commonly known as drometrizole. Drometrizole and its phenyl substituents are potent UV-light absorbers and constitute an important class of industrial additives for polymers and light-stabilized coatings. They are used in a variety of polymers including polycarbonates, unsaturated polyesters, polystyrenes, acrylics, polyvinyl chloride, thermoplastic polyesters, and polyacetals. They have the common photochemical feature of strong absorption of ultraviolet light (290–350 nm). This feature, as an ultraviolet absorber (UVA), is utilized commercially to impart light stability (protection against photo-degradation) to a wide variety of polymers (plastics, polyesters, celluloses, acrylates, dyes, rubber, synthetic and natural fibers, waxes, detergent solutions, and orthodontic adhesives) against discoloration and deterioration [1].

Dugdale and Cotton [2] has reported that benzotriazole forms a strongly bonded chemisorbed two-dimensional barrier film less than 50 Å thick, which may be a monomolecular layer, protects copper and its alloys in aqueous media, various atmospheres, lubricants, and hydraulic fluids [2]. Moreover, benzotriazole forms insoluble precipitates with copper ions in solution, thereby preventing the corrosion of aluminum and steel in other parts of a water system [2].

The UV-stabilizer 2-(2′-hydroxy-5′-methylphenyl)-benzotriazole (Hhmbt) has been reported as a ligand for complexing VO^{2+} and MoO_2^{2+} to give [{VO(acac)$_2$}(μ-hbmt)$_2$] and *cis*-[MoO_2(acac)(hmbt)]. The X-ray crystal structures of both of complexes have been also discussed [3]. The photolability of Hhmbt was explained due to an excited-state intramolecular proton transfer through the intramolecular hydrogen bond (Form A, B; Scheme 1) [4–6]. Thus, the replacement with a transition metal (chelates the oxygen and nitrogen) with the investigation of its effect on the photochemical and photophysical properties have been reported [3].

The complexes, [$ReOX_2$(hmpbta)(APh_3)]·MeCN (X = Cl, Br; A = P, As) and [$ReBr_2$(hmpbta)(PPh_3)]·MeCN (hmpbta = 2-(2′-hydoxy-50-methylphenyl)-benzotriazole), have been prepared and characterized. The X-ray structure and DFT calculations for the disubstituted [ReOCl(hmpbta)$_2$] chelate have also been reported [7].

Over the past few years, our laboratory has been actively involved in the synthesis of O,O; O,N; N,S and O,N,S-donors transition metal complexes, which have been evaluated as anticancer agents against either *Ehrlich ascites* tumor cells (EACs) [8–11] or human cancer cell lines [12–14]. As a continuation of our interest in complexes with O,N-donors [8,12,15–17], here we describe the preparation and characterization of new Zn(II), MoO_2^{2+}, Ru(II), Rh(III), Pd(II), Ag(I), Pt(II) complexes with 2-(2′-hydroxy-5′-methylphenyl)-benzotriazole (Hhmbt) as simple or primary ligand and 2,2′-bipyridyl, 9,10-phenanthroline or triphenylphosphine as secondary ligands. The anticancer activity of Hhmbt and its complexes have been tested against human breast cancer (MDA-MB231) and human ovarian cancer (OVCAR-8) cell lines.

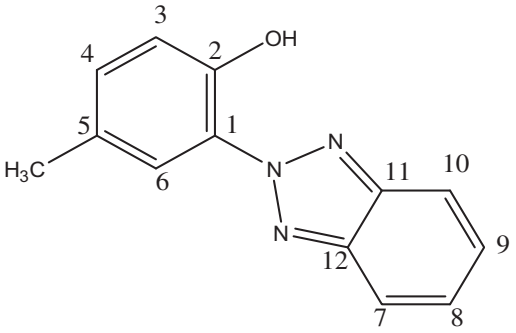

Fig. 1. Structure of 2-(2′-hydroxy-5′-methylphenyl)-benzotriazole (Hhmbt).

2. Experimental

2.1. Materials and measurements

All reagents and solvents were purchased from Alfa/Aesar and all manipulations were performed under aerobic conditions using materials and solvents as received. [M(bpy)Cl_2], [M(phen)Cl_2], [M(PPh_3)$_2Cl_2$] (M(II) = Pd, Pt) [18] and [Ru(PPh_3)$_3Cl_2$] [19]. DMSO-d_6 was used for the NMR measurements referenced against TMS.

The human breast cancer (MDA-MB231) and human ovarian cancer (OVCAR-8) cell lines were obtained from the American Type Culture Collection (ATCC catalog number). Cells were maintained in Dulbecco's Modified Eagle Medium (Wisent Inc., St-Bruno, Canada) supplemented with 10% FBS, 10 mM HEPES, 2 mM L-gutamine and 100 μg/mL penicillin/streptomycin (GibcoBRL, Gaithersburg, MD). In all assays cells were plated 24 h before drug treatment.

Infrared spectra were recorded on a Nicolet 6700 Diamond ATR spectrometer in the 4000–200 cm^{-1} range. NMR spectra were recorded on VNMRS 200 and 500 MHz spectrometer in DMSO-d_6 using TMS as reference. Mass spectra (ESI-MS) were recorded using LCQ Duo and double focusing MS25RFA instruments, respectively. Electronic spectra were recorded in DMF using a Hewlett-Packard 8453 spectrophotometer. Thermal analysis measurements were made in the 20–800 °C range at a heating rate of 20 °C min^{-1} using Ni and NiCo as references, on a TA instrument TGA model Q500Analyzer TGA-50. Molar conductivity measurements were carried out at room temperature on a YSI Model 32 conductivity bridge.

2.2. Preparations

2.2.1. [Pd(hmbt)(H_2O)Cl]·2H_2O

An aqueous solution of $K_2[PdCl_4]$ (0.16 g, 0.5 mmol; 5 mL) was added to Hhmbt (0.113 g, 0.5 mmol) in EtOH (15 mL). The resulting suspension was stirred at 80 °C for 2 h and a yellow solid was obtained. It was filtered off, washed with water, ethanol and air-dried. Yield: 0.195 g, 71%. *Elemental Anal.:* Calcd. C, 37.1; H, 3.8; N, 10.0; Pd, 25.3 ($C_{13}H_{16}N_3O_4Pd$); Found: C, 37.2; H, 3.9; N, 10.3; Pd, 25.4%. Conductivity data (10^{-3} M in DMF): Λ_M = 8.0 ohm^{-1}. IR (cm^{-1}): ν(C=N), 1600; ν(CO), 1250; ν(N–N), 1141; ν(Pd–O), 501; ν(Pd–N), 461. Raman (cm^{-1}): ν(C=N), 1573; ν(CO), 1251; ν(N–N), 1149; ν(Pd–O), 538; ν(Pd–N), 471; ν(Pd–Cl), 194. ^{1}H NMR (ppm): 7.96 (H(3), d, *J* = 3 Hz, 1H); 7.65 (H(6), S, 1H); 7.23 (H(7), d, *J* = 4.5 Hz, 1H); 7.40 (H(8), t, *J* = 4.2 Hz, 1H); 7.30 (H(9), t, *J* = 4.2 Hz, 1H); 7.08 (H(10), d, *J* = 4.5 Hz, 1H); 2.40 (CH3, S, 3H). UV–visible (nm): 248, 386, 468. MS (*m*/*z*): 331 (Calcd. 330.4), 226 (Calcd. 226.4).

2.2.2. [Pd(hmbt)$_2$]

An aqueous solution of $K_2[PdCl_4]$ (0.16 g, 0.5 mmol; 5 mL) was added to Hhmbt (0.225 g, 1 mmol) in MeOH containing KOH (0.056 g, 1 mmol; 15 mL). The reaction mixture was stirred at 45° C for 2 h. The orange solid was filtered off, washed with water, ethanol and air-dried. Yield: 0.320 g; 83%. *Elemental Anal.:* Calcd. C, 56.3; H, 3.6; N, 15.2; Pd, 19.2 ($C_{26}H_{20}N_6O_2Pd$); Found: C, 56.1; H, 3.5; N, 15.3; Pd, 19.1%. Conductivity data (10^{-3} M in DMF): Λ_M = 5.0 ohm^{-1}. IR (cm^{-1}): ν(C=N), 1612; ν(CO), 1251; ν(N–N), 1141; ν(Pd–O), 501; ν(Pd–N), 473. Raman (cm^{-1}): ν(C=N), 1572; ν(CO), 1251; ν(N–N), 1148; ν(Pd–O), 538; ν(Pd–N), 471. UV–visible (nm):278, 388. MS (*m*/*z*): 554.5 (Calcd. 554.4), 329.4 (Calcd. 330.4), 226.7 (Calcd. 226.4).

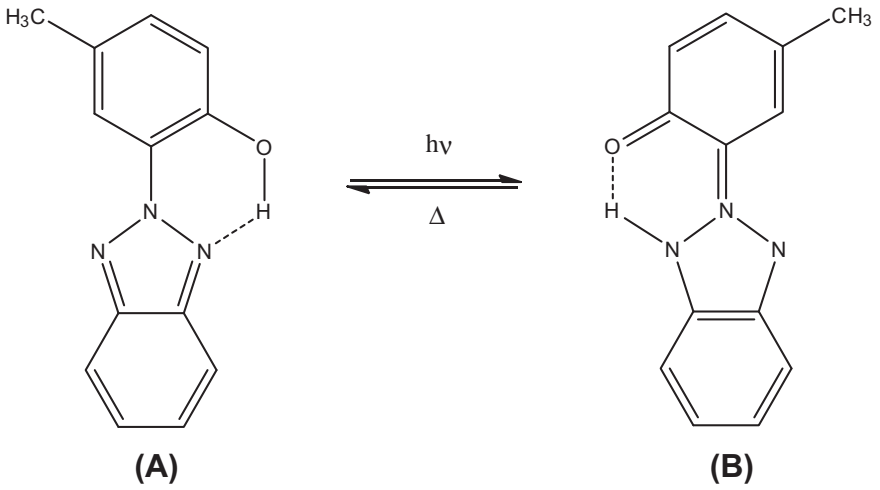

Scheme 1. Enol-keto tautomeric (A and B) forms of Hhmbt.

2.2.3. [Pd(L)(hmbt)]Cl·nH$_2$O (L = bpy, n = 2; L = phen, n = 1)

To a stirred suspension of [Pd(bpy)Cl$_2$] (0.03 g, 0.1 mmol) or [Pd(phen)Cl$_2$] (0.04 g, 0.1 mmol) in MeOH (10 mL) a solution of Hhmbt (0.023 g, 0.1 mmol) in MeOH containing KOH (0.006 g, 0.1 mmol; 10 mL) was added drop by drop with stirring. The reaction mixture was warmed for 48 h, upon which a yellow-orange precipitate was filtered off, washed with MeOH, Et$_2$O and dried in *vacuo*.

For[Pd(bpy)(hmbt)]Cl·2H$_2$O: Yield: 0.07 g (51%). *Elemental Anal.:* Calcd. C, 49.5; H, 4.3; N, 12.6; Pd, 19.1 ($C_{23}H_{24}N_5O_3Pd$); Found: C, 49.7; H, 4.2; N, 12.7; Pd, 19.1%. Conductivity data (10^{-3} M in DMF): Λ_M = 84.0 ohm^{-1}. IR (cm^{-1}): ν(C=N), 1621; ν(CO), 1251; ν(N–N), 1141; ν(Pd–O), 500; ν(Pd–N), 459. Raman (cm^{-1}): ν(C=N), 1602; ν(CO), 1251; ν(N–N), 1141; ν(Pd–O), 501; ν(Pd–N), 460. ^{1}H NMR (ppm): 8.00 (H(3), d, *J* = 6 Hz, 1H); 7.75 (H(6), S, 1H); 7.86 (H(7), d, *J* = 5.4 Hz, 1H); 7.73 (H(8), t, *J* = 5 Hz, 1H); 7.69 (H(9), t, *J* = 5 Hz, 1H); 7.22 (H(10), d, *J* = 5.2 Hz, 1H); 2.50 (CH3, S, 3H). MS (*m*/*z*): 486.4 (Calcd. 486.4), 368.2 (Calcd. 368.4), 292.4 (Calcd. 292.4), 262.4 (Calcd. 262.4), 156.3 (Calcd. 156.0).

For[Pd(phen)(hmbt)]Cl·H$_2$O: Yield: 0.08 g (54%). *Elemental Anal.:* Calcd. C, 53.2; H, 3.9; N, 12.4; Pd, 18.7 ($C_{25}H_{22}N_5O_2Pd$); Found: C, 53.3; H, 4.0; N, 12.3; Pd, 18.6%. Conductivity data (10^{-3} M in DMF): Λ_M = 81.0 ohm^{-1}. IR (cm^{-1}): ν(C=N), 1600; ν(CO), 1252; ν(N–N), 1138; ν(Pd–O), 564; ν(Pd–N), 495. Raman (cm^{-1}): ν(C=N), 1604; ν(CO), 1252; ν(N–N), 1139; ν(Pd–O), 565; ν(Pd–N), 495. ^{1}H NMR (ppm): 7.96 (H(3), d, *J* = 5.1 Hz, 1H); 7.30 (H(6), S, 1H); 7.60 (H(7), d, *J* = 4.5 Hz, 1H); 7.77 (H(8), t, *J* = 4.2 Hz, 1H); 7.73 (H(9), t, *J* = 4.5 Hz, 1H); 7.22 (H(10), d, *J* = 4.2 Hz, 1H); 2.50 (CH3, S, 3H). MS (*m*/*z*): 510.4 (Calcd. 510.4), 286.4 (Calcd. 286.4), 180.6 (Calcd. 180.0).

2.2.4. [Pd(PPh$_3$)(hmbt)Cl]

[Pd(PPh$_3$)$_2$Cl$_2$] (0.175 g, 0.25 mmol) was added to Hhmbt (0.057 g, 0.25 mmol) in CH$_2$Cl$_2$ (20 mL). The reaction mixture was heated under reflux for 48 h. The yellow precipitate was filtered off, washed with CH$_2$Cl$_2$ and dried in *vacuo*. Yield: 0.20 g; 86%. *Elemental Anal.:* Calcd.: C, 59.2; H, 4.0; N, 6.7; Cl, 5.7; Pd, 16.9 ($C_{31}ClH_{25}N_3OPd$); Found: C, 59.4; H, 4.1; N, 6.6; Cl, 5.6; Pd, 16.8%. Conductivity data (10^{-3} M in DMF): Λ_M = 7.0 ohm^{-1}. IR (cm^{-1}): ν(C=N), 1586; ν(CO), 1307; ν(N–N), 1158; ν(Pd–O), 532; ν(Pd–N), 438. Raman (cm^{-1}): ν(C=N), 1585; ν(CO), 1309; ν(N–N), 1160; ν(Pd–O), 530; ν(Pd–N), 434; ν(Pd–P), 301; ν(Pd–Cl), 199. UV–visible (nm): 280, 358, 388. MS (*m*/*z*): 628.2 (Calcd. 627.9).

2.2.5. [Pt(L)(hmbt)]Cl·nH$_2$O (L = bpy, n = 1; L = phen, n = 2)

A similar procedure as the palladium analogue was applied, [Pt(L)Cl$_2$] (L = bpy, phen) were used to produce yellow-orange precipitates.

For [Pt(bpy)(hmbt)]Cl·H$_2$O: Yield: 0.35 g (60%). *Elemental Anal.:* Calcd.: C, 43.9; H, 3.5; N, 11.1; Pt, 31.0 ($C_{23}ClH_{22}N_5O_2Pt$); Found: C, 43.7; H, 3.7; N, 11.0; Pt, 31.2%. Conductivity data (10^{-3} M in DMF): Λ_M = 80.0 ohm^{-1}. IR (cm^{-1}): ν(C=N), 1607; ν(CO), 1251; ν(Pt–O), 549; ν(Pt–N), 489. Raman (cm^{-1}): ν(C=N), 1605; ν(CO), 1251; ν(Pt–O), 550; ν(Pt–N), 486. ^{1}H NMR (ppm): 8.34 (H(3), d, *J* = 5.1 Hz, 1H); 7.68 (H(6), S, 1H); 7.49 (H(7), d, *J* = 4.8 Hz, 1H); 7.2 (H(8), t, *J* = 6.3 Hz,1H); 7.55 (H(9), t, *J* = 5.4 Hz, 1H); 6.76 (H(10), d, *J* = 6 Hz, 1H); 2.35 (CH3, S, 3H). MS (*m*/*z*): 574.3 (Calcd. 574.0).

For [Pt(phen)(hmbt)]Cl·2H$_2$O: Yield: 0.1 g (60%). *Elemental Anal.:* Calcd.: C, 46.0; H, 3.7; N, 10.7; Pt, 29.9 ($C_{25}ClH_{24}N_5O_3Pt$); Found: C, 46.1; H, 3.8; N, 10.5; Pt, 29.7%. IR (cm^{-1}): ν(C=N), 1600; ν(CO), 1251; ν(N–N), 1134; ν(Pt–O), 549; ν(Pt–N), 473. Raman (cm^{-1}): ν(C=N), 1605; ν(CO), 1251; ν(N–N), 1136; ν(Pt–O), 550; ν(Pt–N), 476. Conductivity data (10^{-3} M in DMF): Λ_M = 79.0 - ohm^{-1}. ^{1}H NMR (ppm): 7.96 (H(3), d, *J* = 3.9 Hz, 1H); 7.59 (H(6), S, 1H); 7.06 (H(7), d, *J* = 1.8 Hz, 1H); 7.45 (H(8), t, *J* = 3.3 Hz, 1H); 7.42 (H(9), t, *J* = 3.3 Hz, 1H); 6.85 (H(10), d, *J* = 8.4 Hz, 1H); 2.35 (CH3, S, 3H). MS (*m*/*z*): 599.5 (Calcd. 599.0).

2.2.6. [Pt(PPh$_3$)(hmbt)Cl]

The synthesis of [Pt(PPh$_3$)(hmbt)Cl] was achieved by a similar procedure to that for Pd(II) analogue with [Pt(PPh$_3$)$_2$Cl$_2$] replacing[Pd(PPh$_3$)$_2$Cl$_2$]. Yield: 0.21 g (82%). *Elemental Anal.:* Calcd.: C, 51.9; H, 3.5; N, 5.9; Cl, 5.0; Pt, 27.2 ($C_{31}ClH_{25}N_3OPt$); Found: C, 51.4; H, 3.6; N, 6.0; Cl, 5.4; Pt, 27.5%. Conductivity data (10^{-3} M in DMF): Λ_M = 3.0 ohm^{-1}. IR (cm^{-1}): ν(C=N), 1600; ν(CO), 1300; ν(N–N), 1132; ν(Pt–O), 514; ν(Pt–N), 492. Raman (cm^{-1}): ν(C=N), 1598; ν(CO), 1301; ν(N–N), 1144; ν(Pt–O), 545; ν(Pt–N), 462; ν(Pt–P), 305; ν(Pt–Cl), 227. MS (*m*/*z*): 716.5 (Calcd. 716.5).

2.2.7. [Ag$_2$(hmbt)$_2$]

Silver nitrate (0.085 g, 0.5 mmol) in water (1 mL) was added to Hhmbt (0.113 g, 0.5 mmol) in MeOH containing KOH (0.028 g, 0.5 mmol; 15 mL). The reaction mixture was stirred at 40 °C in the dark for 5 h. The pale-green solid was filtered off, washed with water, MeOH, Et$_2$O and dried in *vacuo*. Yield: 0.15 g (75%). *Elemental Anal.:* Calcd. C, 47.0; H, 3.0; N, 12.6% ($C_{26}H_{20}N_6O_2Ag_2$); Found: C, 47.3; H, 3.2; N, 12.4%. Conductivity data (10^{-3} M in DMF): Λ_M = 6.0 ohm^{-1}. IR (cm^{-1}): ν(C=N), 1600; ν(CO), 1250; ν(N–N),

1144; ν(Ag–O), 500; ν(Ag–N), 465. Raman (cm^{-1}): ν(C=N), 1598; ν(CO), 1250; ν(N–N), 1147; ν(Ag–O), 502; ν(Ag–N), 464. MS (*m*/*z*): 332.22 (Calcd. 331.8).

2.2.8. [Ag(phen)(hmbt)]

Silver perchlorate (0.101 g, 0.5 mmol) in water (1 mL) was added to phen (0.090 g, 0.5 mmol) in MeOH (10 mL). To the yellow solution, Hhmbt (0.113 g, 0.5 mmol) in MeOH containing KOH (0.028 g, 0.5 mmol; 10 mL) was added. The reaction mixture was stirred in the dark for 3 h and the pale-yellow solid was filtered off, washed with water, MeOH, Et_2O and dried in *vacuo*. Yield: 0.21 g (72%). *Elemental Anal.:* Calcd. C, 58.6; H, 3.9; N, 13.7% ($C_{25}H_{20}N_5OAg$); Found: C, 58.9; H, 3.8; N, 13.6%. Conductivity data (10^{-3} M in DMF): Λ_M = 4.0 ohm^{-1}. IR (cm^{-1}): ν(C=N), 1590, ν(CO), 1250; ν(N–N), 1141; ν(Ag–O), 514; ν(Ag–N), 440. Raman (cm^{-1}): ν(C=N), 1589, ν(CO), 1250; ν(N–N), 1143; ν(Ag–O), 553; ν(Ag–N), 418. UV–visible (nm): 225, 269, 288, 441. MS (*m*/*z*): 511.3 (Calcd. 511.8), 287.3 (Calcd. 287.8).

2.2.9. [Ag(PPh_3)(hmbt)]

A similar procedure as [Ag(phen)(hmbt)] was applied, PPh_3 was replacing phen to produce a green precipitate. Yield: 0.29 g (86%). *Elemental Anal.:* Calcd. C, 61.0; H, 4.4; N, 6.9% ($C_{31}H_{27}N_3O_2PAg$); Found: C, 60.7; H, 4.4; N, 7.0%. Conductivity data (10^{-3} M in DMF): Λ_M = 2.0 ohm^{-1}. IR (cm^{-1}): ν(C=N), 1609; ν(CO), 1250; ν(N–N), 1141; ν(Ag–O), 501; ν(Ag–N), 461. Raman (cm^{-1}): ν(C=N), 1607; ν(CO), 1250; ν(N–N), 1147; ν(Ag–O), 509; ν(Ag–N), 464. ^1H NMR (ppm): 7.96 (H(3), d, *J* = 4 Hz, 1H); 7.65 (H(6), S, 1H); 7.31 (H(7), d, *J* = 3.5 Hz, 1H); 7.40 (H(8), t, *J* = 8.5 Hz, 1H); 7.30 (H(9), t, *J* = 4.5 Hz, 1H); 6.73 (H(10), d, *J* = 8.5 Hz, 1H); 2.47 (CH3, S, 3H). UV–visible (nm): 257, 280, 339, 416. MS (*m*/*z*): 593.4 (Calcd. 593.8), 369.4 (Calcd. 369.8).

2.2.10. [Rh(hmbt)$_2$(H_2O)$_2$]Cl·5H_2O

Hydrated rhodium trichloride (0.13 g, 0.5 mmol) was added to a solution of AcONa (0.62 g, 7.5 mmol) in water (30 mL) and Hhmbt(0.226 g, 1.0 mmol) was added. The mixture was refluxed for 10 h and a yellow precipitate was obtained upon reducing the volume. It was filtered off, washed with ice-cold water and air dried. Yield: 0.35 g (60%). *Elemental Anal.:* Calcd.: C, 43.8; H, 4.3; N, 11.8 ($C_{26}H_{35}N_6O_7Rh$); Found; C, 43.8; H, 4.2; N, 11.7%. Conductivity data (10^{-3} M in DMF): Λ_M = 79.0 ohm^{-1}. IR (cm^{-1}): ν(C=N), 1604; ν(CO), 1251; ν(N–N), 1146; ν(Rh–O), 506; ν(Rh–N), 471. Raman (cm^{-1}): ν(C=N), 1602; ν(CO), 1251; ν(N–N), 1148; ν(Rh–O), 497; ν(Rh–N), 476. ^1H NMR (ppm): 8.01 (H(3), d, *J* = 2.8 Hz, 1H); 7.62 (H(6), S, 1H); 7.21 (H(7), d, *J* = 2 Hz, 1H); 7.52 (H(8), t, *J* = 6 Hz, 1H); 7.50 (H(9), t, *J* = 5.6 Hz, 1H); 7.06 (H(10), d, *J* = 4.4 Hz, 1H); 2.48 (CH3, S, 3H). UV–visible (nm): 280, 310, 358, 408, 430. MS (*m*/*z*): 551.2 (Calcd. 551.0).

2.2.11. [Ru(hmbt)$_2$(H_2O)$_2$]

Hydrated ruthenium trichloride (0.102 g, 0.5 mmol) in water (5 mL) was added to Hhmbt (0.34 g, 1.5 mmol) in EtOH (15 mL). The mixture was heated under reflux for 6 h till a dark green precipitate formed. It was filtered off during hot, washed with hot water, EtOH and air dried. Yield: 0.35 g (80%). *Elemental Anal.:* Calcd.: C, 53.3; H, 4.3; N, 14.2 ($C_{26}H_{24}N_6O_3Ru$); Found; C, 53.5; H, 4.1; N, 14.4%. Conductivity data (10^{-3} M in DMF): Λ_M = 5.0 ohm^{-1}. IR (cm^{-1}): ν(C=N), 1611; ν(CO), 1251; ν(N–N), 1137; ν(Ru–O), 501; ν(Ru–N), 468. Raman (cm^{-1}): ν(C=N), 1611; ν(CO), 1251; ν(N–N), 1143; ν(Ru–O), 502; ν(Ru–N), 467. UV–visible (nm): 300, 340, 631. MS (*m*/*z*): 549.9 (Calcd. 549.1).

2.2.12. [Ru(PPh_3)(hmbt)$_2$Cl]

A stirred suspension of [Ru(PPh_3)$_3$$Cl_2$] (0.25 g, 0.25 mmol) in MeOH (10 mL) was added to a Hhmbt (0.09 g, 0.4 mmol) in MeOH (10 mL). The reaction mixture was heated under reflux for 2 h during which shiny green microcrystals were isolated, washed with MeOH, Et_2O and dried in *vacuo*. Yield: 0.26 g (83%). *Elemental Anal.*: Calcd.: C, 62.4; Cl, 4.2; H, 4.1; N, 9.9 ($C_{44}ClH_{35}N_6O_2PRu$); Found: C, 62.5; Cl, 4.1; H, 4.4; N, 10.0%. Conductivity data (10^{-3} M in DMF): Λ_M = 4.0 ohm^{-1}. IR (cm^{-1}): ν(C=N), 1633; ν(CO), 1255; ν(N–N), 1131; ν(Ru–O), 519; ν(Ru–N), 438. Raman (cm^{-1}): ν(C=N), 1619; ν(CO), 1262; ν(N–N), 1133; ν(Ru–O), 531; ν(Ru–N), 420. UV–visible (nm): 305, 362, 629. MS (*m*/*z*): 811.2 (Calcd. 811.1), 588.0 (Calcd. 587.1).

2.2.13. [Zn(hmbt)(OAc)(H_2O)$_2$]

$Zn(OAc)_2$ (0.109 g, 0.5 mmol) in EtOH (5 mL) was added to Hhmbt (0.113 g, 0.5 mmol) in EtOH (20 mL). The reaction mixture was heated under reflux for 8 h. A pale-yellow precipitate was obtained, washed with EtOH and dried in *vacuo*. Yield: 0.18 g (81%). *Elemental Anal.*: Calcd.: C, 46.9; H, 4.0; N, 10.9 ($C_{15}H_{17}N_3O_5Zn$); Found: C, 47.1; H, 4.2; N, 11.0%. Conductivity data (10^{-3} M in DMF): Λ_M = 9.0 ohm^{-1}. IR (cm^{-1}): ν(C=N), 1615; ν(CO), 1250; ν(N–N), 1132; ν(Zn–O), 520; ν(Zn–N), 441. Raman (cm^{-1}): ν(C=N), 1612; ν(CO), 1258; ν(N–N), 1131; ν(Zn–O), 548; ν(Zn–N), 459. ^1H NMR (ppm): 8.06 (H(3), d, *J* = 3.3 Hz, 1H); 7.56 (H(6), S, 1H); 7.31 (H(7), d, *J* = 6 Hz, 1H); 7.55 (H(8), t, *J* = 6 Hz, 1H); 7.52 (H(9), t, *J* = 5.7 Hz, 1H); 6.73 (H(10), d, *J* = 7.5 Hz, 1H); 2.47 (CH3, S, 3H). MS (*m*/*z*): 384.3 (Calcd. 384.5), 366.2 (Calcd. 366.5).

2.2.14. [Zn(hmbt)$_2$(H_2O)$_2$]

$ZnCl_2$ (0.11 g, 0.5 mmol) in water (5 mL) was added to Hhmbt (0.225 g, 1 mmol) in EtOH containing (0.028 g, 0.5 mmol; 20 mL). The reaction mixture was heated under reflux for 4 h. An off-white precipitate was obtained. It was filtered off, washed with water, EtOH and dried in *vacuo*. Yield: 0.29 g (87%). *Elemental Anal.*: Calcd.: C, 60.8; H, 3.9; N, 16.4 ($C_{26}H_{20}N_6O_2Zn$); Found: C, 61.0; H, 3.8; N, 16.3%. Conductivity data (10^{-3} M in DMF): Λ_M = 11.0 - ohm^{-1}. IR (cm^{-1}): ν(C=N), 1613; ν(CO), 1252; ν(N–N), 1132; ν(Zn–O), 500; ν(Zn–N), 463. Raman (cm^{-1}): ν(C=N), 1612; ν(CO), 1250; ν(N–N), 1130; ν(Zn–O), 504; ν(Zn–N), 464. ^1H NMR (ppm): 8.00 (H(3), d, *J* = 2.8 Hz, 1H); 7.64 (H(6), S, 1H); 7.64 (H(7), d, *J* = 4.4 Hz, 1H); 7.21 (H(8), t, *J* = 4.4 Hz, 1H); 7.52 (H(9), t, *J* = 6.4 Hz, 1H); 7.50 (H(10), d, *J* = 3.6 Hz, 1H); 2.47 (CH3, S, 3H). MS (*m*/*z*): 513.1 (Calcd. 513.5), 289.1 (Calcd. 289.5).

2.2.15. Cis-[MoO_2(hmpt)$_2$]

[MoO_2(acac)$_2$] (0.164 g, 0.5 mmol) in methanol (2 mL) was added HL_1 (0.225 g, 1 mmol) in methanol containing KOH (0.028 g, 0.5 mmol; 10 mL). The reaction mixture was heated under reflux for 3 h. The pale yellow precipitate was filtered off, washed with water and methanol, and finally air-dried. Yield:0.089 g (23%). *Elemental Anal.*: Calcd.: C, 54.2; H, 3.5; N, 14.6 ($C_{26}H_{20}N_6O_4Mo$); Found: C, 54.5; H, 3.6; N, 14.7%. Conductivity data (10^{-3} M in DMF): Λ_M = 4.0 ohm^{-1}. IR (cm^{-1}): ν(C=N), 1604; ν(CO), 1253; ν(N–N), 1145; ν(O–Mo–O), 939; ν(Mo–O), 560; ν(Mo–N), 470. Raman (cm^{-1}): ν(C=N), 1606; ν(CO), 1250; ν(N–N), 1149; ν(O–Mo–O), 942; ν(Mo–O), 570; ν(Mo–N), 473. ^1H NMR (ppm): 7.98 (H(3), d, *J* = 7 Hz, 1H); 7.02 (H(6), S, 1H); 7.54 (H(7), d, *J* = 7.5 Hz, 1H); 7.16 (H(8), t, *J* = 3.5 Hz, 1H); 7.52 (H(9), t, *J* = 5 Hz, 1H); 7.19 (H(10), d, *J* = 3.5 Hz, 1H); 2.47 (CH3, S, 3H). MS (*m*/*z*): 575.8 (Calcd. 575.9), 352.1 (Calcd. 351.9).

2.3. Biological assay

Growth inhibition assay; human breast cancer (MDA-MB231) and human ovarian cancer (OVCAR-8) cells were plated at 3000 cells/well in 96-well (100 μL/well) flat-bottomed microliter plates (Costar, Corning, NY). After 24 h incubation, the cells were exposed to different concentrations of each compound continuously for

5 days. Briefly, following drug treatment, the cells were fixed using 50 μL of cold trichloroacetic acid (50%) for 2 h at 4 °C, washed with water, stained with sulforhodamine B (SRB 0.4%) overnight at room temperature, rinsed with 1% acetic acid and allowed to dry overnight [20]. The resulting colored residue was dissolved in 200 μL Tris base (10 mM, pH 10.0) and the optical density was recorded at 490 nm using a microplate reader ELx808 (BioTek Instruments). The results were analyzed by GraphPad Prism (GraphPad Software, Inc., San Diego, CA) and the sigmoidal dose response curve was used to determine 50% cell growth inhibitory concentration (IC_{50}). Each point represents the average of two independent experiments performed in triplicate [20].

3. Result and discussion

Section 2 describes the synthesis of the new complexes of 2-(2′-hydroxy-5′-methylphenyl)-benzotriazole (Hhmbt) and lists their elemental analyses and spectroscopic data, which are in excellent agreement with the assigned formulae. The molar conductivities (Λ_M) in DMF at room temperature suggest all complexes to be non-electrolytes except for,[M(L)(hmbt)]Cl (M(II) = Pd, Pt; L = bpy, phen) and $[Rh(hmbt)_2(H_2O)_2]Cl$, which show as 1:1 electrolytes [21]. All the new complexes are microcrystalline or powder-like, stable under normal laboratory conditions and soluble in DMF and DMSO.

3.1. Vibrational spectra

The solid-state properties of 2-(2′-hydroxy-5′-methylphenyl)-benzotriazole (Hhmbt; Fig. 1) were examined by IR and Raman spectroscopy. The spectrum of Hhmbt was compared with those of the complexes. Tentative assignments of selected IR bands are reported in the experimental section. The IR spectrum of Hhmbt exhibits a strong broad at band at 3400 cm^{-1} due to ν(OH), support the existence of Hhmbt in the enol form (Scheme 1) [3,7], this band is missed on the complexes. These data are further supported by the shift of the intense band near 1250 cm^{-1} in the spectra of free ligand to higher frequency, indicating the coordination of Hhmbt through the deprotonated phenolic (C(2)–O^-) [22,23]. These observations indicate the replacement of the acidic hydrogen by the metal ion [13]. The strong band at 1600 (IR) and 1601 (Raman) cm^{-1} in free ligand is characteristic of ν(C=N) group. It is expected that coordination of the nitrogen to the metal ion would reduce the electron density in the azomethine link and thus shifted ν(C=N) stretch [24]. In the spectra of the complexes, this band is shifted to the region at 1604–1630 cm^{-1} [25]. The band near 1131 cm^{-1} in free Hhmbt is assigned to the ν(N–N) stretch. In the complexes, this band is shifted to lower wave number [26]. These means that $hmbt^-$ acts as a mononegative bidentate ligand, coordinating the metal ions through the azomithine nitrogen and the deprotonated hydroxy oxygen centers forming six-membered ring. In the complex, $[Zn(hmbt)(AcO)(H_2O)_2]$ (Fig. 2), two extra bands are observed at 1532 and 1408 cm^{-1} assigned to $\nu_{as}(COO^-)$ and $\nu_s(COO^-)$ stretching vibration of the acetate group, respectively [15]. The separation between these two bands {$\Delta = \nu_{as}(COO^-)$ and $\nu_s(COO^-) = 124\ cm^{-1}$}, indicating asymmetric bidentate coordination of the carboxylic group [15,16].

The presence of the coordinated PPh_3 groups in $[M(hmbt)(PPh_3)Cl]$ (M(II) = Pd, Pt), $[Ru(PPh_3)(hmbt)_2Cl]$ and $[Ag(PPh_3)(hmbt)(H_2O)]$ is manifested by the strong IR bands near 1099 and 751 cm^{-1}, attributed to the $\nu(P–C_{ph})$ and δ(C–CH) vibrations, respectively [27].

The spectra of the complexes, [M(L)(hmbt)]Cl (M(II) = Pd, Pt; L = bpy, phen) show bands near 1580, 1515, 1495, 1420 (phen) and 854, 841, 750 and 725 (bpy) cm^{-1} are attributed to the γ(CH) vibrations of the coordinated phen or bpy [15,28]. These bands are at higher wavenumbers compared with those for the free phen or bpy ligand indicating chelation [29].

In the 1000–750 cm^{-1} region, the spectra of $[MoO_2(hmbt)_2]$ (Fig. 3) shows bands characteristic of the *cis*-MoO_2^{2+} units [30,31]. The IR bands at 939 (943 in Raman) and 897 (911 in Raman) cm^{-1} are assigned to the $\nu_s(MoO_2)$ and $\nu_{as}(MoO_2)$ modes, respectively [30,31]. As expected, the symmetric mode is weak in the IR spectra and strong in Raman, while the opposite applies for the asymmetric one. The appearance of two stretching bands is indicative of the *cis*-configuration [15,32,33].

The IR and Raman spectra of the complexes show several bands in 500–200 cm^{-1} due to ν(M–O), ν(M–N), ν(M–P) and ν(M–Cl) stretches [26,33].

3.2. NMR spectra

The ^1H NMR spectroscopic data for Hhmbt complexes in DMSO-d_6 are reported in the experimental section.

The spectrum of the free Hhmbt (see Fig. 1 for numbering scheme) exhibits three singlets at δ 3.34, 7.69 and 10.35 ppm attributed to CH_3, H(6) and OH, respectively. There are two triplets at δ 7.55 and 7.52 ppm and four doublets at δ 8.03, 8.00, 7.24 and 7.05 ppm assigned to H(8), H(9), H(3), H(4), H(7) and H(10), respectively. The sharp singlet due to OH proton, is missed in the complexes, indicating the replacement of the hydroxy proton by the metal ions [34]. On the other hand, the signals for H(7) and H(10) are shifted downfield, indicating the complexation of $hmbt^-$ through the deprotonated hydroxy oxygen and imine nitrogen atoms [35,36].

The ^1H NMR spectrum of $[Rh(hmbt)_2(H_2O)_2]Cl$ should show the presence of *fac* and *mer* isomers since $hmbt^-$ is an unsymmetrical bidentate ligand (imine and deprotonated hydroxy oxygen atoms are non-equivalent). In the *fac* isomer, the $hmbt^-$ are equivalent while in the *mer* they are different [10,37]. Two peaks are observed for each proton assigned to *cis*-$hmbt^-$ and *cis*-H_2O configuration (Fig. 4). This feature was further supported by ^{13}C NMR spectrum, and expected due to the bulky $hmbt^-$ moieties.

The ^1H NMR spectra of the $[M(hmbt)(PPh_3)Cl]$, $[M(hmbt)(L)]Cl$ (M(II) = Pd, Pt; L = bpy, phen), $[Ag(PPh_3)(hmbt)(H_2O)]$ and $[Ru(PPh_3)(hmbt)_2Cl]$ complexes show complicated multiplets in the δ 7.6–8.4 and 7.2–7.8 ppm regions, which are assigned to bpy or phen and PPh_3 protons, respectively. The bpy or phen and PPh_3 protons show upfield shifts in comparison to those of $[M(L)Cl_2]$ (M(II) = Pd, Pt; L = bpy, phen) and $[Ru(PPh_3)_3Cl_2]$. This observation is interpreted in term of strong binding of $hmbt^-$ to metal ions as compared to binding of chloride ion [9].

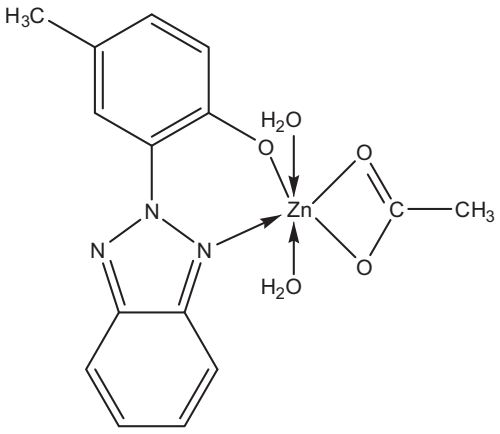

Fig. 2. Structure of $[Zn(hmbt)_2(H_2O)_2]$.

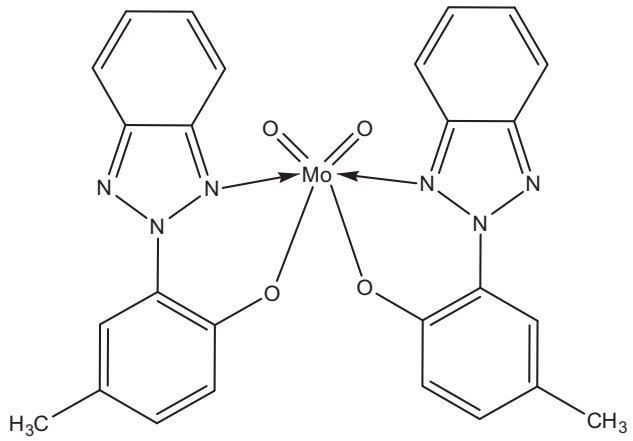

Fig. 3. Structure of *cis*-[MoO_2(hmbt)$_2$].

The ^{31}P NMR spectra of the complexes, [M(hmbt)(PPh_3)Cl] (M(II) = Pd, Pt), [Ag(PPh_3)(hmbt)] and[Ru(hmbt)$_2$(PPh_3)Cl] in DMSO-d_6 show sharp singlet near δ 20.0 ppm, suggesting the presence of one coordinated PPh_3 moiety in the complex [38].

The ^{13}C NMR spectrum of Hhmbt in DMSO-d_6 has been measured and assigned. The spectrum shows ten resonances at δ 20.28, 118.24, 118.37, 125.36, 127.14, 127.80, 129.11, 132.04, 143.88 and 148.88 ppm, may be assigned to CH_3(5), C(3), C(8,9), C(4), C(6), C(7,10), C(1), C(5), C(11,12) and C(2), respectively. In the complexes, the resonances for the carbon atoms adjacent to the coordination sites, C(1), C(2), C(3), C(11) and C(12), are shifted downfield relative to their positions in the free ligand (Table 1) [39]. This feature may be due to an increase in the benzotriazole ring current in C(11) and C(12) brought about by coordination to triazole nitrogen center [18]. In the spectrum of [Rh(hmbt)$_2$(H_2O)$_2$]Cl, two signals were observed for each carbon atom, supporting the *cis*-configuration, which observed in the ^{1}H NMR spectrum.

3.3. Electronic spectra

The electronic spectra of Hhmbt in EtOH and DMSO show three bands near 250, 300 and 358 nm. The electronic spectra of the complexes in H_2O, MeOH, DMSO or Nujol in the 200–900 nm regions contain intense bands due to ligand to metal charge-transfer (LMCT) transitions and weaker bands assigned to d–d transitions

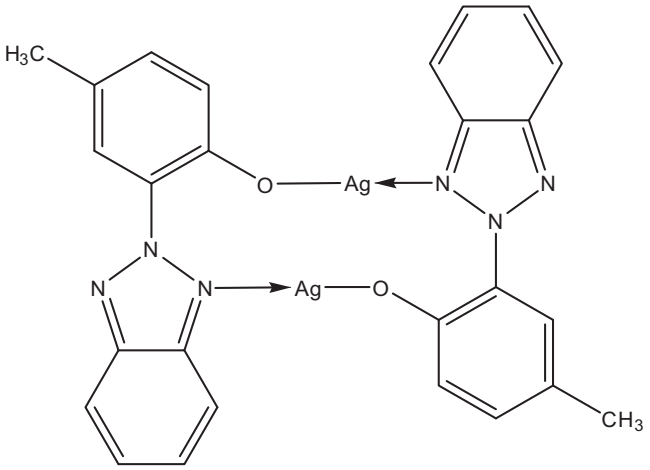

Fig. 4. Structure of [Ag_2(hmbt)$_2$].

[40]. Transitions below 400 nm are assigned to intra-ligand charge transfer (n → π^* and $\pi \rightarrow \pi^*$).

The electronic spectrum of the diamagnetic complex, [Rh(hmbt)$_2$(H_2O)$_2$]Cl, display bands at 589, 497 and 408 nm, which resemble those of other octahedral Rh(III) complexes and may be assigned to $^1A_{1g} \rightarrow {}^3T_{1g}$, $^1A_{1g} \rightarrow {}^1T_{1g}$ and $^1A_{1g} \rightarrow {}^1T_{2g}$ transitions, respectively [10,32,41].

The electronic spectra of the diamagnetic ruthenium (II) complexes show intense transitions near 636 ($^1A_{1g} \rightarrow {}^1T_{1g}$), 340 ($^1A_{1g} \rightarrow {}^1T_{2g}$) and 300 (ligand ($\pi$–d$\pi$)) nm [10]. These are attributed to a low-spin octahedral geometry around Ru(II) [8,10]. The electronic spectra of the diamagnetic Pd(II), Pt(II) complexes exhibit bands near 470 and 320 nm due to $^1A_{1g} \rightarrow {}^1B_g$ and $^1A_{1g} \rightarrow {}^1E_g$ transitions, respectively, in a square-planar configuration [42,43]. In the complexes, [M(hmbt)(PPh_3)Cl], [M(hmbt)(L)]Cl (M(II) = Pd, Pt; L = bpy, phen), the absorption band at 370 nm is assigned to a mixture of charge transfer from M(II) to the π^* orbital of bpy, phen or PPh_3 and d–d bands [10,42,43].

In the electronic spectrum of complex *cis*-[MoO_2(hmbt)$_2$] displays bands at 456 and 358 (shoulder) nm; the latter is assigned to $O^{2-} \rightarrow$ Mo(VI) p–d transition and is characteristic of the MoO_2^{2-} moiety in octahedral geometry [10].

3.4. Mass spectra

The mass spectral data of the complexes are reported in the Experimental section and their molecular ion peaks are in agreement with their assigned formulae.

The mass spectrum of [Pd(hmbt)(H_2O)Cl] shows fragmentation patterns corresponding to successive degradations of the molecule. The first signal at *m*/*z* 331 (Calcd. 330.4) with 50% abundance represents the molecular ion, [Pd(hmbt)]$^+$. The spectrum exhibits one more peak at 226.0 (Calcd. 226.4) corresponding to [Pd(hmbt-$C_6H_4N_2$)]$^+$. The mass spectrum of [Pd(hmbt)$_2$] shows the first peak at *m*/*z* 554.5 (Calcd. 554.4) with 100% abundance corresponding to [Pd(hmbt)$_2$]$^+$. The spectrum exhibits two more peaks at 329.4, 226.7 corresponding to [Pd(hmbt)]$^+$, [Pd(hmbt-$C_6H_4N_2$)]$^+$ fragments, respectively. The mass spectra of [Pd(bpy)(hmbt)]Cl and [Pd(phen)(hmbt)]Cl show peaks at *m*/*z* 486.4, 510.4, respectively, represent the molecular ions [Pd(bpy)(hmbt)]$^+$ (Calcd. 486.4) and [Pd(phen)(hmbt)]$^+$ (Calcd. 510.4), respectively. The mass spectrum of [M(hmbt)(PPh_3)Cl] (M(II) = Pd, Pt) show signals at *m*/*z* 628.2 (Calcd. 627.9), Pd and 716.5 (Calcd. 716.5), Pt, in agreement with the molecular ions [M(hmbt)(PPh_3)Cl]$^+$. The fragmentation pattern of Pt(II) complex indicates the stepwise ligand loss to [Pt(PPh_3)]$^{2+}$ (457) [8]. The mass spectra of [Pt(bpy)(hmbt)]Cl and [Pt(phen)(hmbt)]Cl show peaks at *m*/*z* 574.3 and 599.5, represent the molecular ions [Pt(bpy)(hmbt)]$^+$ (Calcd. 575.0) and [Pd(phen)(hmbt)]$^+$ (Calcd. 599.0), respectively.

The mass spectrum of the complex, [Zn(hmbt)$_2$(H_2O)$_2$] shows the first signal at *m*/*z* 513.1 (Calcd. 513.5) with 100% abundance corresponding to the molecular ion [Zn(hmbt)$_2$]$^+$. One more signal at 289.1 (Calcd. 289.5) is associated with [Zn(hmbt)]$^+$ fragment, indicating step wise ligand loss [43].

The spectrum of [Rh(hmbt)$_2$(H_2O)$_2$]Cl shows signal at 551.2 (Calcd. 551.1) corresponding to the molecular ion [Rh(hmbt)$_2$]$^+$. The spectrum of [Ru(hmbt)$_2$(H_2O)$_2$] shows a signal at *m*/*z* 549.9 (Calcd. 549.1) corresponding to [Ru(hmbt)$_2$]$^+$ [8] while that of [Ru(PPh_3)(hmbt)$_2$Cl] shows peaks at *m*/*z* 812.2 and 588.0, which correspond to [Ru(PPh_3)(hmbt)$_2$]$^+$ (Calcd. 811.1) and [Ru(PPh_3)(hmbt)]$^+$ (Calcd. 587.1), respectively, in agreement with step wise ligand loss [10].

The spectrum of [Ag_2(hmbt)$_2$] (Fig. 4) shows signal *m*/*z* at 332.2 (Calcd. 331.8) with 8% abundance corresponding to [Ag(hmbt)]$^+$. The signal at 291.2 (Calcd. 289.8) is associated with [Ag(hmbt-N_3)]$^+$ fragment. The spectrum of [Ag(PPh_3)(hmbt)] shows peaks

Table 1
^{13}C NMR spectral data of Hhmbt and its complexes.

Compounds	C1	C2	C3	C4	C5	C6	C7	C8	C9	C10	C11	C12	CH_3
					δ ppm								
Hhmbt	129.11	148.88	118.24	125.36	132.04	127.14	127.80	118.37	118.37	127.80	143.88	143.88	20.28
[Pd(hmbt)(H_2O)Cl]	132.00	152.00	118.98	125.67	132.32	127.43	127.98	119.04	119.18	129.30	148.43	148.56	21.09
[Rh(hmbt)$_2$(H_2O)$_2$]Cl[a]	131.54	152.90	118.56	125.89	132.33	127.40	127.99	119.32	119.55	129.32	147.90	148.29	21.11
	131.80	153.06	118.81	126.06	132.61	127.56	128.24	119.49	119.84	129.73	148.12	148.55	21.36
[Zn(hmbt)(OAc)(H_2O)$_2$]	131.82	153.00	118.43	125.68	132.21	127.78	128.80	119.00	119.87	129.06	148.76	149.04	22.01
[Zn(hmbt)$_2$(H_2O)$_2$]	132.41	154.04	118.61	125.54	132.25	127.65	128.41	119.73	119.79	128.98	147.99	148.87	21.98
Cis-[MoO_2(hmpt)$_2$]	131.23	153.81	118.78	125.59	132.09	127.88	128.00	119.09	119.68	129.07	148.31	148.97	20.98

[a] Two signals for each C indicating *cis*-(hmbt$^-$)$_2$ configuration.

at *m*/*z* 593.4 and 369.3, corresponding to [Ag(PPh_3)(hmbt)]$^+$ (Calcd. 593.8) and [Ag(PPh_3)]$^+$ (Calcd. 369.8) fragments, respectively.

3.5. Thermal measurements

The thermal stability and degradation behaviour of some of the reported complexes, [Zn(hmbt)(OAc)(H_2O)$_2$], [Zn(hmbt)$_2$], [Pd(hmbt)(H_2O)Cl]·3H_2O, [Pd(hmbt)$_2$], [Pd(hmbt)(PPh_3)Cl], [M(bpy)(hmbt)]Cl (M = Pd, *n* = 2; M = Pt, *n* = 1), [M(phen)(hmbt)]Cl (M = Pd, *n* = 1; M = Pt, *n* = 2), *cis*-[MoO_2(hmbt)$_2$], [Ag$_2$(hmbt)$_2$], [Ag(PPh_3)(hmbt)], [Ru(hmbt)$_2$(H_2O)$_2$], [Ru(PPh_3)(hmbt)$_2$Cl] and [Rh(hmbt)$_2$(H_2O)$_2$]-Cl·5H_2O, were studied using the thermogravimetric (TG) technique. The weight loss observed below 130 °C is due to dehydration as the colours changed from pale to deeper [37,41].

The thermogram of [Zn(hmbt)(OAc)(H_2O)$_2$], shows the first-step weight loss of 28.9% between 196 and 272 °C, which corresponds to the release of two coordinated waters molecules per molecule of complex, AcO and ½N_2 (Calcd. 29.1%). The second decomposition occurs between 272 and 359° C, which is attributed to the loss of C_7H_6 and $C_6H_4N_2$ fragments (Calcd. 50.5, Found 50.9%), leaving ZnO (21.2%). The thermogram of [Zn(hmbt)$_2$(H_2O)$_2$] shows TG inflection in the ranges 150–470 °C, arise from the release of two coordinated water, 2$C_7H_6N_3$ and C_6H_4O fragments (Calcd. 71.3, Found 70.7%), leaving ZnO as a residue.

The thermogram of [Pd(hmbt)(H_2O)Cl]·3H_2O, shows the first-step weight loss of 13.3% between 63 and 110 °C, which corresponds to the release of three waters molecules (Calcd. 12.3%); the relatively low temperature shows that these water molecules are crystal lattice held [9,10,41]. Another endothermic decomposition occurs between 111 and 350 °C, which is attributed to the loss of coordinated H_2O, ½ Cl_2 and C_6H_4 fragment (Calcd. 29.6, Found 29.4%) [27]. There is other TG inflection in 350–610 °C region, may arise from the elimination of $C_7H_6N_3$ (Calcd. 30.2, Found 30.5%) fragment, leaving PdO (28.0%). The thermogram of [Pd(hmbt)$_2$], is characterized by two steps in 225–425 and 426–575 °C region. They are assigned to the elimination of $C_{13}H_{11}N_3$, $C_6H_4N_3$ (Calcd. 58.8, Found 59.1%) and C_7H_6O (Calcd. 19.1, Found 18.8%), fragments, respectively, leaving PdO residue at 700° C (22.1%) [27]. The thermogram of [Pd(bpy)(hmbt)]Cl·2H_2O shows the first endothermic weight loss between 23 and 150 °C, may be due to the release of crystal lattice water and ½ Cl_2 molecule (Calcd. 12.8, Found 12.8%). The second decomposition step occurs between 151 and 350 °C, attributed to the loss of bpy species (Calcd. 28.0, Found 28.2%). The second TG inflection between 351 and 450 °C may arise from the elimination of $C_6H_4N_3$ fragment (Calcd. 21.2, Found 21.3%), leaving PdO (Calcd. 21.9%). The thermogram of [Pd(phen)(hmbt)]Cl·H_2O shows weight losses in the 23–150, 151–270, 271–580 and 581–900° C, which may correspond to the release of crystal lattice water (Cacld. 3.2, Found 3.5%), ½ Cl_2 and $C_7H_6N_2$ species (Calcd. 27.2, Found 27.5%), ½ N_2 and C_6H_4N(Calcd. 21.0, Found 21.1%) and $C_{12}H_{10}$ (Calcd. 27.0, Found 26.5%) fragments, leaving PdO (18.21%). The thermogram of [Pt(phen)(hmbt)]Cl.2H_2O, is characterized by three steps in 30–100, 101–300 and 301–650 °C regions. These are assigned to the elimination of lattice water (Calcd. 5.3, Found 5.1%), ½ Cl_2, phen and C_4H_4 (Calcd. 39.9, Found 40.1%), $C_9H_6N_3$ (Calcd. 23.3, Found 22.9%), fragments, respectively, leaving PtO residue at 700 °C (31.4%) [10,27]. The thermogram of [Pt(bpy)(hmbt)]Cl·H_2O shows the first endothermic weight loss between 35 and 150 °C, which may correspond to the release of crystal lattice water and ½ Cl_2 (Cacld. 8.5, Found 8.2%). The second decomposition step occurs between 151 and 320 °C, attributed to the loss of C_6H_4N fragment (Calcd. 14.3, Found 14.6%) while the third one between 321 and 589 °C arise from the elimination of N_2 and phen species (Calcd. 33.1, Found 33.1%). The fourth TG inflection lies in the 590–700 °C range, arise from the release of C_7H_6 fragment (Calcd. 14.3, found 13.9%), leaving PtO (Calcd. 33.6, Found 34.6%).

The TGA data for the complex, [Rh(hmbt)$_2$(H_2O)$_2$]Cl·5H_2O, shows three TG inflections in the ranges 65–213, 214–301 and 302–431 °C. The first weight loss may arise from the release of five water of crystallization, two molecule water of coordination, ½ Cl_2 and $C_6H_4N_3$ fragments (Calcd. 39.2, Found 39.5%), C_6H_4 fragments (Calcd. 10.6, found 10.3%) and $C_7H_6N_3O_{½}$ (Calcd. 19.7, Found 19.8%), respectively, leaving Rh_2O_3 as a residue at 700 °C (17.8%).

For the complex, [Ru(hmbt)$_2$(H_2O)$_2$]·2H_2O, four TG inflections in the ranges 60–180, 181–350, 351–450 and 451–600 °C were observed. The first one arise from the release of two water of crystallization and two water of coordination (Calcd. 11.6, Found 11.8%), 2N_2 molecules (Calcd. 9.0, Found 8.7%), C_6H_4N and C_6H_4 fragments (Calcd. 26.7, Found 27.0%), and C_7H_6N and C_7H_6 fragments (Calcd. 32.5, Found 32.4%), respectively, leaving Ru_2O_3 as a residue at 700 °C (20.1%). The thermogram of [Ru(PPh_3)(hmbt)$_2$Cl], show three TG inflections in the ranges 217–304, 305–389 and 390–588 °C, arise from the release of ½ Cl_2 (Calcd. 4.2, Found 4.3%), $C_7H_6N_3$ fragment (Calcd. 15.6, found 15.5%), 3Ph fragments (Calcd. 27.3, found 26.9%), and C_6H_4 and $C_7H_6N_2$ fragments (Calcd. 22.9, found 22.6%) respectively [33], leaving Ru_2O_3 as a residue at 700 °C (15.7%).

The thermogram of [Ag$_2$(hmbt)$_2$], shows the first-step weight loss of 24.9% between 175 and 275 °C, may be attributed to the release of 2C_6H_4, ½ N_2 (Calcd. 25.0%). The second step occurs between 276 and 430 °C, attributed to the loss of C_6H_4, N_2 and ½ N_2 (Calcd. 17.7, Found 17.1%). The last decomposition step occurs between 431–510 °C, attributed to the loss of $C_7H_6N_2O$ (Calcd. 20.1, Found 19.7%), leaving Ag_2O (34.9%). The complex, [Ag(PPh_3)(hmbt)], shows two TG inflections in the ranges 175–310 and 311–900 °C, arised from the release of PPh_3 and $C_6H_4N_3$ fragments (Calcd. 63.9, Found 63.9%), and $C_7H_6O_{½}$ fragment (Calcd. 16.5, Found 16.8%), leaving Ag_2O as a residue (19.5%) [12].

3.6. Anticancer activity

Cis-platin is considered to be one of the best known small metal-containing drug molecules. It acts as anticancer agent for

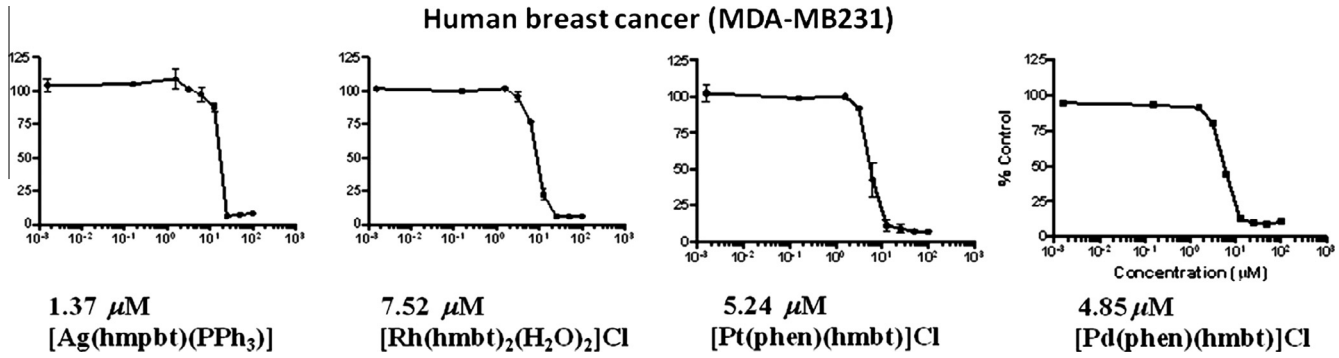

Fig. 5A. IC_{50} values of [Ag(hmpbt)(PPh_3)], [Rh(hmbt)$_2$(H_2O)$_2$]Cl, [Pt(phen)(hmbt)]Cl and [Pd(phen)(hmbt)]Cl tested against the human breast cancer (MDA-MB231) cell lines.

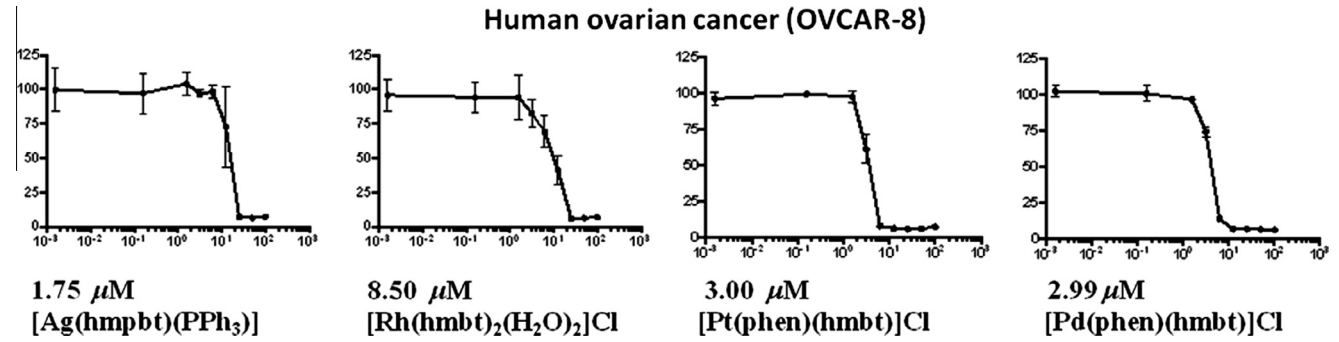

Fig. 5B. IC_{50} values of [Ag(hmpbt)(PPh_3)], [Rh(hmbt)$_2$(H_2O)$_2$]Cl, [Pt(phen)(hmbt)]Cl and [Pd(phen)(hmbt)]Cl tested against the human ovarian cancer (OVCAR-8) cell lines.

several human cancers, particularly, testicular and ovarian cancers [8–14]. Generally, the side effects, especially nephrotoxicity, limit its widespread use in high doses [44]. The need to develop new complexes with reduced nephrotoxicity and higher activity has stimulated the synthesis of many new complexes. Over the past years, a renewed interest in Zn(II), Ag(I), Pd(II) and Pt(II) complexes as potential anticancer agents has developed in our laboratory [8–14].

We have recently examined the *in vitro* anticancer activity of DL-piperidine-2-carboxylic acid (DL-H_2pa) and its complexes, *trans*-[Zn_2(μ-Ca)$_2$(Hpa)$_2$$Cl_6$], [Pd(bpy)(Hpa)]Cl and [M(pa)(PPh_3)$_2$] against serous ovarian cancer ascites, OV 90 cell line [12]. The ultimate goal of this research is to develop new complexes with high efficacy against cancer cells. The *in vitro* anticancer activity of the free Hhmbt and its complexes, [Zn(hmbt)$_2$(H_2O)$_2$], [Zn(hmbt)(OAc)(H_2O)$_2$], [M(bpy)(hmbt)]Cl, [M(phen)(hmbt)]Cl (M(II) = Pd, Pt), [Ag_2(hmbt)$_2$], [Ag(PPh_3)(hmbt)] and [Rh(hmbt)$_2$(H_2O)$_2$]Cl were tested against the human breast cancer (MDA-MB231) and human ovarian cancer (OVCAR-8) cell lines in comparison to *cis*-platin as a reference (Fig. 5; Table 2). The complexes, [Ag_2(hmbt)$_2$], [Ag(hmpbt)(PPh_3)], [Rh(hmbt)$_2$(H_2O)$_2$]Cl, [Pt(phen)(hmbt)]Cl and [Pd(phen)(hmbt)]Cl exhibit the highest growth inhibitory activity with mean IC_{50} values 14.13, 1.37, 7.52, 5.24 and 4.85 μM (MDA-MB231) and 13.54, 1.75, 8.50, 3.00 and 2.99 μM (OVACAR-8), respectively; the IC50 values of *cis*-platin being 32.00 and 30.86 μM.

Generally, it is accepted that binding of *cis*-platin to genomic DNA (g-DNA) in the cell nucleus is the main event responsible for its antitumor properties [45]. Thus, the damage induced upon binding of cisplatin to g-DNA may inhibit transcription, and/or DNA replication mechanisms. Subsequently, these alterations in DNA processing would trigger cytotoxic processes that lead to cancer cell death. An important property of Pt(II) complexes is the fact that Pt–ligand bonds (Pt–N, Pt–O, Pt–P), which have the thermodynamic strength of a typical coordination bond, are much weaker than C–C, C–N or C–O covalent bonds; the data obtained from TGA analysis, discussed above, confirming this feature. However, the ligand exchange behavior in Pt complexes is quite slow, which gives them high kinetic stability. Thus, the ligand exchange reactions take place in minutes to days, rather than microseconds to seconds as in case of Pd(II) complexes [46]. The high activity of the complexes, [Ag_2(hmbt)$_2$] and [Ag(hmpbt)(PPh_3)], is expected, since Ag(I) complexes have been reported as active anti-cancer agents and wound healing stimulators [13,47]. In addition, the pulk PPh_3 group and its slow hydrolysis may explain the activity of the later complex with respect to the first one [9,10]. Moreover, the kinetic *trans* effect is responsible for ligand exchange reactions; i.e., donor atoms located *trans* to other donors with strong *trans* effect are more rapidly substituted than ligands in *cis*-positions [46]. These features may explain the activity of [Pt(phen)(hmbt)]Cl (Fig. 6) and [Pd(phen)(hmbt)]Cl complexes, which may attribute

Table 2
Anticancer activity of Hhmbt and its complexes against the human breast cancer (MDA-MB231) and human ovarian cancer (OVCAR-8) cell lines.

Compounds	IC_{50} (μM) Human breast cancer (MDA-MB231) cell lines	IC_{50} (μM) Human ovarian cancer (OVCAR-8) cell lines
Hhmbt	>100	87.55
[Zn(hmbt)$_2$(H_2O)$_2$]	>100	84.69
[Zn(hmbt)(OAc)(H_2O)$_2$]	37.75	33.20
[Pd(bpy)(hmbt)]Cl	45.96	37.37
[Pt(bpy)(hmbt)]Cl	18.89	23.54
[Pd(phen)(hmbt)]Cl	4.85	2.99
[Pt(phen)(hmbt)]Cl	5.24	3.00
[Ag_2(hmbt)$_2$]	14.13	13.54
[Ag(PPh_3)(hmbt)]	1.37	1.75
[Rh(hmbt)$_2$(H_2O)$_2$]Cl	7.52	8.50
Cis-platin	32.0	30.86

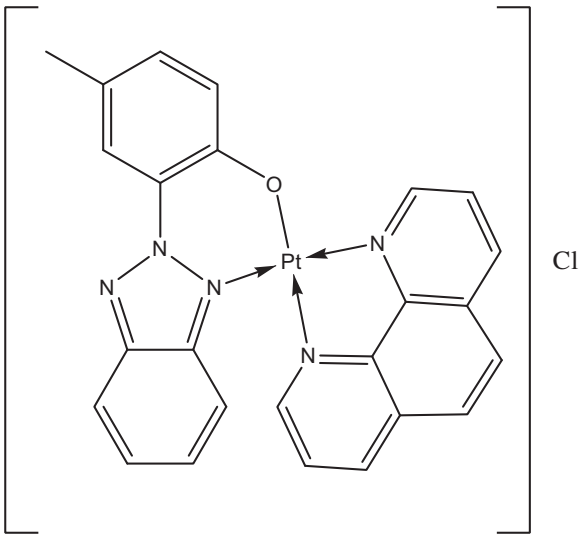

Fig. 6. Structure of [Pt(hmbt)(phen)]Cl.

to their square-planar geometry, the slow hydrolysis of the bulk phen donor as well as its *cis*-N,N-donor nature, and the high conductivity and solubility of these complexes [9–12]. The complexes, $[Ag_2(hmbt)_2]$, [Ag(hmpbt)(PPh_3)], [Pt(phen)(hmbt)]Cl and [Pd(phen)(hmbt)]Cl show high efficacy towards the human breast cancer (MDA-MB231) and human ovarian cancer (OVCAR-8) cell lines. In addition, they are high promising anticancer agents towards these cancers, especially they show very low toxicity toward normal human breast and ovarian cell lines. For the complex, $[Rh(hmbt)_2(H_2O)_2]$Cl, its activity may be attributed to its solubility as well as the low reactivity; i.e., the slow ligand exchange reaction [47]. The water soluble complexes, [Pt(bpy)(hmbt)]Cl {IC_{50} 18.89 μM (MDA-MB231) and 23.54 μM (OVACAR-8)} and [Pd(bpy)(hmbt)]Cl {IC_{50} 45.96 μM (MDA-MB231) and 37.37 μM (OVACAR-8)} show moderate activity. On the other hand, the low activity of the other complexes, $[Zn(hmbt)_2(H_2O)_2]$, $[Zn(hmbt)(OAc)(H_2O)_2]$ and $[Ag_2(hmbt)_2]$ may be came from their poor solubility, difficulty in hydrolysis to produce their cationic form or fast interaction with DNA under physiological conditions [47].

4. Conclusions

New complexes of Hhmbt with Zn(II), Pd(II), Pt(II), Ag(I), Ru(II), Rh(III), MoO_2^{2+}, WO_2^{2+} and UO_2^{2+} have been synthesized and characterized. Hhmbt behaves as a mononegative bidentate through the deprotonated phenolic oxygen and imine nitrogen atoms. The complexes, [Ag(hmpbt)(PPh_3)], $[Rh(hmbt)_2(H_2O)_2]$Cl, [Pt(phen)(hmbt)]Cl and [Pd(phen)(hmbt)]Cl, show promissing activity against human breast cancer (MDA-MB231) and human ovarian cancer (OVCAR-8) cell lines.

Acknowledgements

We are grateful to the Ministry of Higher Education in Egypt (H. El-Asmy) and a NSERC (Canada) Discovery grant (ISB) for the financial support of this work.

Appendix A. Supplementary material

Supplementary data associated with this article can be found, in the online version, at http://dx.doi.org/10.1016/j.molstruc.2013.11.039.

References

[1] M. Chanda, S.K. Roy, Plastic Technology Handbook, fourth ed., Plastic Engineering Series, CRC Press, 2010.
[2] I. Dugdale, J.B. Cotton, Corros. Sci. 3 (1963) 69–74.
[3] T. Carofiglio, E. Solari, C. Floriani, Polyhedron 15 (1996) 4435–4440.
[4] H.J. Heller, H.R. Blattman, Pure Appl. Chem., Some aspects of the light protection of polymers 30 (1972) 145–146; Some aspects of stabilization of polymers against light 36 (1973) 141–148; H.J. Heller, Eur. Polym. J. (Suppl. 5) (1969) 105–114.
[5] W. K1opfer, in: J.N. Pitts, S.S. Hammond, K. Gallnick (Eds.), Advances in Photochemistry, vol. 10, Wiley, New York, 1977, p. 311. and refs therein; D.L. Williams, A. Heller, J. Phys. Chem. 74 (1974) 4473–4480; J.E.A. Otterstedt, J. Phys. Chem. 58 (1973) 5716–5725.
[6] G. Wosner, G. Goeller, J. Rieker, H. Hoier, J.J. Sterowski, E. Daltrozzo, M. Neurieter, E.A. Kramer, J. Phys. Chem. 89 (1985) 3629–3636; G. Wosner, G. Goeller, J. Rieker, H. Hoier, J.J. Sterowski, E. Daltrozzo, M. Neurieter, E.A. Kramer, J. Phys. Chem. 88 (1984) 5544–5550.
[7] B. Machura, M. Wolff, R. Kruszynski, J. Kusz, Polyhedron 28 (2009) 1211–1220; B. Machura, M. Wolff, D. Tabak, J.A. Schachner, N.C. Mösch-Zanetti, Eur. J. Inorg. Chem. (2012) 3764–3773.
[8] I. Gabr, H. El-Asmy, M. Emmam, S.I. Mostafa, Transition Met. Chem. 34 (2009) 409–418.
[9] S.I. Mostafa, Transition Met. Chem. 32 (2007) 769–775.
[10] S.I. Mostafa, J. Coord. Chem. 61 (2008) 1553–1567.
[11] S.I. Mostafa, F.A. Badria, Met.-Based Drugs (2008) 1–7, http://dx.doi.org/10.1155/2008/723634.
[12] A.A. Alie El-Deen, A.E. El-Askalany, R. Halaoui, B.J. Jean-Claude, I.S. Butler, S.I. Mostafa, J. Mol. Struct. 1036 (2013) 161–167.
[13] S. El-Sayed, B. Jean, J. Mol. Struct. 1028 (2012) 208–214.
[14] S.A. Elsayed, A.M. El-Hendawy, S.I. Mostafa, B.J. Jean-Claude, M. Todorova, I.S. Butler, Bioinorg. Chem. Appl. (2010), http://dx.doi.org/10.1155/2010/149149 (1-11).
[15] A. Ouf, M.S. Ali, E.M. Saad, S.I. Mostafa, J. Mol. Struct. 973 (2010) 69–75.
[16] A. Ouf, M.S. Ali, M.S. Sulyman, A.M. El-Defrawy, S.I. Mostafa, J. Korean Chem. Soc. 54 (2010) 402–410.
[17] N.A. Anaan, E.M. Saad, S.M. Hassan, I.S. Butler, S.I. Mostafa, Carbohydr. Res. 346 (2011) 775–793.
[18] W.P. Griffith, S.I. Mostafa, Polyhedron 11 (1992) 2997–3005.
[19] R.I. Kureshy, N.H. Khan, S.H. Abdi, P. Tyer, J. Inorg. Nucl. Chem. 28 (1966) 945–956.
[20] P. Skehan, R. Storeng, D. Scudiero, J. Natl Cancer Inst. 82 (1990) 1107–1112.
[21] W. Geary, Coord. Chem. Rev. 7 (1971) 81–122.
[22] V.M. Leovac, L.S. Jovanovic, L.J. Bjelica, V.I. Cesljevic, Polyhedron 8 (1989) 135–141.
[23] M.F. El-Shazly, T. Salem, M.A. El-Sayed, Inorg. Chim. Acta 29 (1978) 155–163.
[24] T.D. Thangadurai, S.K. Ihm, J. Ind. Eng. Chem. 9 (2003) 563–568.
[25] T.D. Thangadurai, K. Natarajan, Transition Met. Chem. 26 (2001) 717–722.
[26] S. Mostafa, A. El-Asmy, M. El-Shahawi, Transition Met. Chem. 25 (2000) 470–473.
[27] S. Mostafa, C. Papatriantafyllopoulou, S. Perlepes, N. Hadjiliadis, Bioinorg. Chem. Appl. (2008), http://dx.doi.org/10.1155/2008/647873.
[28] S. Aruna, G. Shanmugam, Spectrochim. Acta 41A (1985) 531–536.
[29] A.K. Boudalis, V. Nastopoulos, S.P. Perlepes, C.P. Raptopoulou, A. Terzis, Transition Met. Chem. 26 (2001) 276–281.
[30] Z.-H. Zhou, H.-L. Wan, K.-R. Tsai, Inorg. Chem. 39 (2000) 59–64.
[31] H. Arzoumanian, G. Agrifoglio, M.V. Capparelli, R. Atencio, A. Briceño, A. Alvarez-Larena, Inorg. Chim. Acta 359 (2006) 81–89.
[32] S.I. Mostafa, Transition Met. Chem. 23 (1998) 397–401.
[33] K. Nakamoto, Infrared and Raman Spectra of Inorganic and Coordination Compounds, fourth ed., Wiley, New York, 1986.
[34] S.A. Elsayed, A.M. El-Hendawy, I.S. Butler, S.I. Mostafa, J. Mol. Struct. 1036 (2013) 196–202.
[35] S.I. Mostafa, S. Abd El-Maksoud, Monatsh. Chem. 129 (1998) 455–466.
[36] S. Basu, S. Peng, G. Lee, S. Bhattacharya, Polyhedron 24 (2005) 157–163.
[37] S.I. Mostafa, M.M. Bekheit, Chem. Pharm. Bull. Jpn. 48 (2000) 266–271.
[38] M. Tamizh, K. Mereitter, K. Kirchner, B.R. Bhat, R. Karvembu, Polyhedron 28 (2009) 2157–2164.
[39] E. Ainscough, A. Brodie, W. Denny, G. Finlay, J. Ranford, J. Inorg. Biochem. 70 (1998) 175–185.
[40] Y.T. Li, C.W. Jan, Y.J. Zheng, D.Z. Liao, Polyhedron 17 (1998) 1423–1427.
[41] S.I. Mostafa, S.P. Perlepes, N. Hadjiliadis, Z. Naturforsch. 56b (2001) 394–402.
[42] V. Jin, J. Ranford, Inorg. Chim. Acta 304 (2000) 38–44.
[43] S.A. Elsayed, A.M. El-Hendawy, S.I. Mostafa, I.S. Butler, Inorg. Chim. Acta 363 (2010) 2526–2532.
[44] F.P.T. Harmers, W.H. Gispen, J.P. Neijt, Eur. J. Cancer 27 (1991) 372–376.
[45] V. Cepeda, M.A. Fuertes, J. Castilla, C. Alonso, C. Quevedo, J.M. Pérez, Anti-Cancer Agents Med. Chem. 7 (2007) 3–18.
[46] I. Kostova, Recent Pat. Anti-Cancer Drug Discovery I (2006) 1–22.
[47] S.I. Mostafa, I.S. Butler, F. Ibrahim, Y. El-Hawary, CSC2011, Montreal, Canada, 2011; S.I. Mostafa, I.S. Butler, F. Ibrahim, Y. El-Hawary; Eurasia 2012, Corfu, Greece, 2012.